UC Davis

UC Davis Previously Published Works

Title

Junctional sarcoplasmic reticulum motility in adult mouse ventricular myocytes.

Permalink

https://escholarship.org/uc/item/12d7m7zh

Journal

American journal of physiology. Cell physiology, 318(3)

ISSN

0363-6143

Authors

Drum, Benjamin M
Yuan, Can
de la Mata, Ana
et al.

Publication Date

2020-03-01

DOI

10.1152/ajpcell.00573.2019

Peer reviewed

eScholarship.org Powered by the California Digital Library
University of California

Junctional Sarcoplasmic Reticulum Motility in Adult Mouse Ventricular Myocytes

Benjamin M. Drum[1], Can Yuan[1], Ana de la Mata[2], Nathan Grainger[2], and L. Fernando Santana[2]

[1]Department of Physiology and Biophysics, University of Washington, 1704 NE Pacific Street, Seattle, WA, 98195

[2]Department of Physiology & Membrane Biology, University of California, Davis, One Shields Avenue, Davis, CA, 95616

Correspondence to:

LF Santana (lfsantana@ucdavis.edu)

Keywords

Cardiomyocytes; live imaging; junctional sarcoplasmic reticulum; dyadic plasticity; EC coupling

Abbreviations

jSR	Junctional SR
AP	Action potential
EC	Excitation-contraction
TRD-paGFP	Triadin tagged photoactivable-GFP
COV	Coefficient of variation

Downloaded from journals.physiology.org/journal/ajpcell at Univ of California Davis (169.237.094.131) on February 4, 2020.

Abstract

Excitation-contraction (EC) coupling is the coordinated process by which an action potential triggers cardiac myocyte contraction. EC coupling is initiated in dyads where the junctional SR (jSR) is in tight proximity to the sarcolemma of cardiac myocytes. Existing models of EC coupling critically depend on dyad stability to ensure the fidelity and strength of EC coupling, where even small variations in RyR and $Ca_V1.2$ channel separation dramatically alters EC coupling. However, dyadic motility has never been studied. Here, we developed a novel strategy to track specific jSR units in dissociated adult ventricular myocytes using photo-activatable fluorescent proteins. We found that the jSR is not static. Instead, we observed dynamic formation and dissolution of multiple dyadic junctions regulated by the microtubule-associated molecular motors kinesin-1 and dynein. Our data support a model where reproducibility of EC coupling results from the activation of a temporally averaged number of SR Ca^{2+} release units forming and dissolving SR-sarcolemmal junctions. These findings challenge the long-held view that the jSR is an immobile structure and provide insights into the mechanisms underlying its motility.

Downloaded from journals.physiology.org/journal/ajpcell at Univ of California Davis (169.237.094.131) on February 4, 2020.

Introduction

Cardiac contractions are triggered by action potentials (AP). The chain of events that couple an AP to contraction is collectively known as excitation-contraction (EC) coupling. Multiple factors determine the strength of contraction, including Ca^{2+} influx, sarcoplasmic reticulum (SR) Ca^{2+} release, and the sensitivity of contractile proteins to cytosolic Ca^{2+}.

The coefficient of variation of the AP-evoked $[Ca^{2+}]_i$ transient in an adult ventricular myocyte is about 0.1 (21), suggesting high EC coupling reproducibility. To understand mechanisms underlying $[Ca^{2+}]_i$ transient reproducibility, it is pertinent to review key events during EC coupling. Activation of sarcolemmal $Ca_V1.2$ channels during the AP causes a small influx of Ca^{2+} that activates RyRs in the nearby jSR. The small distance and volume separating $Ca_V1.2$ and RyR channels allows even brief openings of $Ca_V1.2$ channels to increase local $[Ca^{2+}]_i$ high enough to activate nearby RyRs. Thus, the fidelity of local EC coupling critically depends on dyad structural stability and hence the separation between RyR and $Ca_V1.2$ channels.

The jSR is a complex structure with several proteins contributing to its architecture and function. Junctophilin-2 (JPH2) is anchored to the jSR in its C-terminus and contacts the sarcolemma through lipid-interacting motifs in its N-terminus (7, 15). JPH2 is hypothesized to provide a molecular bridge between the jSR and the T-tubules (1, 19). The Ca^{2+}-binding protein, calsequestrin is anchored to the jSR membrane by triadin (TRD) and junctin (23). TRD and junctin knockout mice show changes in jSR architecture (8, 23). This is important as even small changes in dyadic size and structure can perturb EC coupling by altering peak $[Ca^{2+}]$ levels and Ca^{2+} decay rates in the dyad (3, 9, 17).

There is growing evidence that the dyad is not a stable structure; T-tubule – SR junctions show dynamic regulation, particularly during disease states (21). Multiple studies show that changes in T-tubule sarcolemma-SR junctions likely contribute to Ca^{2+} instability during pathology. In heart failure, physical uncoupling of the SR and T-tubules (23), T-tubule disorganization (11) and remodeled T-tubules moving away from Z-lines (18) underlie loss of local control and Ca^{2+} instability. Similarly, EC uncoupling and SR network fracturing occur during post-myocardial infarction (22).

However, compared to T-tubule structural studies, jSR plasticity has received little attention. This can be attributed to the ease at which the T-tubule membrane can be visualized and the ineffectiveness of fluorescent labeling of the jSR (10, 21). In this study, we developed a novel strategy to monitor the stability of the T-tubule sarcolemma-SR junction in freshly isolated adult ventricular myocytes. Our data indicate that the jSR is a dynamic structure. This supports a novel paradigm shift that departs from the long-standing model of Ca^{2+} signaling modulated by a static dyad. The dynamic jSR creates another layer of Ca^{2+} signaling regulation; moreover, this regulation could exhibit exquisite local precision.

Results

Expression of TRD-paGFP allows the visualization of the jSR in ventricular myocytes. We designed two AAV9s for specific infection of adult ventricular myocytes: one to express TRD tagged with a photo-activatable GFP (AAV9-TRD-paGFP) and the other a constitutively fluorescent RFP-tag with a retention signal for the SR lumen (SR-RFP) (**Figure 1A**). TRD-paGFP fluorescence is restricted to the set of proteins expressed at the time of photoactivation and is, therefore, proportional to the number of junctional proteins expressed and their relative position within the imaging focal plane.

Downloaded from journals.physiology.org/journal/ajpcell at Univ of California Davis (169.237.094.131) on February 4, 2020.

Isolated ventricular myocytes expressing TRD-paGFP were exposed to the red-shifted potentiometric fluorescent indicator Di-8-ANNEPs (Di-8). Di-8 labeling identifies the sarcolemma and the T-tubular membrane in ventricular myocytes (**Figure 1B**). Upon photoactivation, we observed TRD-paGFP fluorescence in close proximity to Di-8 labeled T-tubules (**Figure 1C**). We analyzed the physical interaction of these signals by calculating a Pearson's co-localization coefficient of 0.95 (C = 10, N = 5). In parallel experiments, myocytes expressing both TRD-paGFP and SR-RFP were photoactivated to validate targeting of TRD-paGFP to the SR. As previously described (21), SR-RFP is broadly expressed in the lumen of the SR, showing that this organelle forms a vast network that extends throughout the cell. Upon photoactivation, TRD-paGFP fluorescence is observed at opposing ends of SR-expressing SR-RFP (**Figure 1D**). Together, these data indicate that TRD-paGFP is expressed and properly targeted to the jSR of ventricular myocytes.

The jSR has multiple modalities of mobility. To assess jSR mobility at T-tubules, we temporally measured and tracked TRD-paGFP and Di-8 signals after photoactivation. Confocal images were acquired in zero-drift compensation mode to ensure stable imaging of the same focal plane. **Movie 1** (https://figshare.com/articles/Movie1_mp4/11396283) shows examples of stable and unstable jSR segments after photoactivation of TRD-paGFP. During analysis, we measured the averaged fluorescence intensity in 0.2 μm diameter ROIs within the area of the cell where TRD-paGFP was photoactivated. Whilst averaging TRD-paGFP intensity, we also determined the time course of Di-8 fluorescence in each of the sites where TRD-paGFP was activated. The coefficient of variation (COV = SD ÷ mean) of all Di-8 labeled sites analyzed had a normal, unimodal distribution (0.021 ± 0.008, C = 14, S = 132, N = 8) (**Figure 2A**). This suggests that T-tubules are stable and that the focal plane did not change during the time course of imaging. In sharp contrast, analysis of TRD-paGFP fluorescent signal COV from these same sites reveals a larger degree of variation in intensities over time, both within and between cells. TRD-paGFP COVs demonstrate a multimodal distribution of fluorescent signals (**Figure 2A**). These distributions could be fit with the sum of four Gaussian functions with centers at 0.06, 0.16, and 0.24 and 0.36 (**Figure 2A**). On the basis of this analysis, we classified jSR sites as "stable" and "unstable". For a jSR to be considered "stable", it must have a COV that is within the mean ± 3 SDs (SD = 0.02) from the lowest TRD-paGFP COV average. Sites with a COV > 0.12, were considered to be "unstable" jSR sites. Figure 2B-G show representative time-courses of TRD-paGFP and Di-8 signals from different imaging sites with variable COV values. In **Figure 2B**, TRD-paGFP and Di-8 fluorescence signals were stable throughout imaging. Indeed, the COV of this site was 0.06 and 0.07 for TRD-paGFP and Di-8, respectively. By contrast, **Figure 2C-D**, show two representative sites displaying TRD-paGFP COVs of 0.18 and 0.25. These relatively unstable sites showed frequent changes in TRD-paGFP, but not Di-8 fluorescence. Some sites demonstrated much greater COV values, suggesting a higher degree of jSR mobility (**Figure 2E-G**).

Because newly synthesized TRD does not fluoresce before activation with UV light, fluorescent intensity fluctuations likely represent changes in the localization of TRD-paGFP proteins previously activated in the experiment. For example, partial changes in TRD-paGFP fluorescence (<100%) likely reflect positional changes of the jSR within the focal plane. We speculate that complete loss and recovery of TRD-paGFP fluorescence is produced by the movement of the jSR in and out the focal plane.

In addition to measuring jSR mobility, we discerned dwell times of jSR at T-tubules (i.e. time Di-8 and TRD-paGFP fluorescent signals overlap). By default, stable TRD-paGFP/jSR sites had membrane dwell times > 15 minutes, or the duration of our experiments. The membrane dwell

Downloaded from journals.physiology.org/journal/ajpcell at Univ of California Davis (169.237.094.131) on February 4, 2020.

times of unstable TRD-paGFP varied from 20-780 seconds, with an average of 257 ± 17.1 seconds (C = 14, N = 8).

We determined three distinct patterns of jSR biogenesis and motility. **Figure 3B** shows exemplary segments of jSR that 1) split to become two distinct segments, 2) retract or withdraw from the T-tubule, or 3) emerge to approach the T-tubule. Images in **Figure 3A** demonstrate a TRD-paGFP signal that split into two distinct segments. Split events represent the minority (15%) of jSR mobility, whereas jSR retraction (57%) and emergence (28%) encompass the majority of movement signatures.

Dynein and kinesin-1 regulate jSR motility and decreases the variance and amplitude of the AP-evoked $[Ca^{2+}]_i$ transient. Work from our lab and others implicates the molecular motors dynein and kinesin-1 in SR/ER motility (14, 21). Dynein drives the processive movement of numerous intracellular cargos towards the minus end of microtubules (2). Kinesin-1 moves unidirectionally toward the plus end of microtubules (12). However, the role of these proteins in jSR mobility is unknown. We packaged motor-less kinesin-1 into viral vectors (AAV9-*Kif5b*DN-RFP) for live cell imaging. We also generated AAV9-*Dnchc1*-shRNA-RFP, which expresses an shRNA directed against *Dnchc1*, encoding dynein. We confirmed successful expression of these viruses by assaying for RFP fluorescence. Expression of this virus reduced dynein mRNA expression by 62%. We found that myocytes expressing *Kif5bDN*-RFP (C = 8, S = 93, N = 5) the median (0.12) and range (0.65) of the COV values of jSR in these cells were lower than those from control myocytes (median = 0.69, range 1.77 ; C = 10, S = 166, N = 4) (**Figure 4A**). Similarly, *Dnchc1*-shRNA-RFP expressing myocytes had a lower median and smaller range of jSR COVs (median = 0.13, range = 0.48 ; C = 9, S = 100, N = 5) than myocytes expressing wild-type *Dnchc1* (median = 0.72, range = 0.1.45; C = 9, S = 148, N = 5). These data suggest that dynein and kinesin-1 regulate jSR mobility in ventricular myocytes.

Finally, we investigated the consequences of disrupting *Kif5b* expression on EC coupling. To do this, we loaded ventricular myocytes expressing *Kif5B*-WT and *Kif5B*-DN with the fluorescent Ca^{2+} indicator Fluo-4-AM and evoked whole-cell $[Ca^{2+}]_i$ transients via field stimulation (1 Hz). During analysis, we aligned and averaged 20 successive $[Ca^{2+}]_i$ transients. **Figure 4B** shows a representative averaged $[Ca^{2+}]_i$ transient from *Kif5B*-WT (C = 7, N = 5) and *Kif5b*-DN (C = 6, N = 4) expressing myocytes. Notably, expression of *Kif5b*-DN decreased the amplitude and the variance of AP-evoked $[Ca^{2+}]_i$ in ventricular myocytes (**Figure 4B**). These data suggest that kinesin-1-dependent movement of the jSR contributes to the fidelity of the $[Ca^{2+}]_i$ transients in ventricular myocytes to elicit EC coupling.

Discussion

This study is the first of its kind to visualize and characterize jSR movement in real time. We have made multiple novel observations relating to cardiac SR dynamics. First, the jSR is dynamic and moves in several modalities. Secondly, this bidirectional mobility is dependent on the molecular motors, kinesin-1 and dynein. Third, jSR mobility contributes to beat-to-beat variability of the AP-evoked $[Ca^{2+}]_i$ in ventricular myocytes. These findings oppose the traditional dogma that the jSR is static to maximize the reproducibility of myocyte response to an AP. Instead, we see a complex system of potential regulation, where jSR segments locally move in and out of the T-tubules. Thus, whilst the reproducibility of the heartbeat under steady-state conditions is perpetuated by local SR Ca^{2+} release from a similar number of couplons in the myocyte, the spatial dwell time of many dyads could be transient.

An intriguing observation in our study is that jSR mobility is multimodal. Interestingly, we find that retraction events are almost twice as common compared to emergence events. Yet, the

Downloaded from journals.physiology.org/journal/ajpcell at Univ of California Davis (169.237.094.131) on February 4, 2020.

number of functional couplons activated during an AP does not change under steady-state conditions, implying that number of jSR emergence and retraction events should be matched (21). How can we reconcile these seemingly contradictory observations? We speculate that while we detected more retractions than emergence events, the average number of functional couplons remains the same under steady-state conditions because the retracting jSR could be replaced by new, non-fluorescent jSR. This could either be a result of a non-photoactivated TRD-paGFP (i.e., initially located outside the field of activation), or by a jSR that only expressed wild-type TRD. Alternatively, retracting jSR with a photoactivated TRD-paGFP could be moving to a different region of the cell, one that is outside the area being imaged.

Several studies provide insights into the potential mechanisms underlying the mobility of the jSR and hence stability of the dyad. JPH2 is necessary for stabilizing the plasmalemma and jSR by providing a structural bridge between membranes. Cardiac-specific disruption of JPH2 expression reduces the number of junctional membranes and increases dyadic size (20). JPH2 can undergo Ca^{2+}-dependent proteolysis under conditions of high $[Ca^{2+}]_i$ in the dyad (13), compromising the coupling between the jSR and plasmalemma. In the context of our findings, we speculate that static jSR segments are stabilized by bound JPH2, whereas mobile jSR, rapidly moving in and out of T-tubules, lacks JPH2. Accordingly, jSR mobility could be related to the number of JPH2 in each dyad.

A second determinant of jSR stability could be the lifetime of $Ca_V1.2$ channel clusters in the dyad. $Ca_v1.2$ clusters are formed by a stochastic self-assembly mechanism in the sarcolemma of ventricular myocytes (16). In developing cardiomyocytes, the nucleocytoplasmic adaptor protein, BIN1 serves as a delivery site for $Ca_V1.2$ channels, thereby facilitating the clustering of $Ca_V1.2$ channels (4). Furthermore, BIN1 serves as an anchor point for the jSR, promoting stable dyads and enhancing EC coupling (4). Thus, the formation of $Ca_V1.2$ clusters in the T-tubular membrane may be the first step in the formation of a functional dyad. Interestingly, the averaged membrane dwell time of mobile jSR that we measured here is similar to that of $Ca_V1.2$ channels (16). Thus, it is intriguing to hypothesize that all elements, including junctophilin, $Ca_V1.2$ channels and BIN1, must be present for a functional, stable dyad to form and that the lifetime of a dyad may be coupled to the lifetime of the associated $Ca_V1.2$ cluster. Further investigations will be required to test this hypothesis.

Another interesting finding in our study is that decreasing jSR mobility by downregulating *Kif5b* expression was associated with a decrease in the variance, but also a decrease in the amplitude of the $[Ca^{2+}]_i$ transient. Thus, jSR mobility may be a determinant of beat-to-beat variability of the $[Ca^{2+}]_i$ transient. At present however, the mechanisms by which loss of *Kif5b* decreases SR Ca^{2+} release are unclear and should be the subject of a future study.

Finally, it is important to note that due to the diffraction-limited resolution of our microscope, we are unable to resolve jSR movement below approximately 250 nm in the lateral axis and 500-600 nm in the axial axis. Therefore, our measurement for jSR mobility or jSR dwell times could be lower level estimates of dyad stability.

In conclusion, our findings suggest a novel mechanism of EC coupling regulation. These studies suggest that jSR mobility may provide another layer of regulation for EC coupling. Future studies are necessary to define the precise extent of jSR mobility, investigate regulatory mechanisms and understand if jSR mobility is disrupted during pathology.

Downloaded from journals.physiology.org/journal/ajpcell at Univ of California Davis (169.237.094.131) on February 4, 2020.

Methods

Isolation of mouse ventricular myocytes. Male mice (C57BL/6J, 6-8 weeks old) were euthanized with a lethal dose of sodium pentobarbital administered intra-peritoneally as approved by the Institutional Animal Care and Use Committee. Ventricular myocytes were isolated using a Langendorff perfusion apparatus as previously described (5). The isolated ventricular myocytes were kept either at room temperature (22 $^{\circ}$C) or at 37°C in Tyrode's solution 0.5–5 h after isolation.

Viral expression system. Mice were anesthetized by isoflurane and injected retro-orbitally with AAV9s encoding the following: TRD tagged with paGFP (AAV9-TRD-paGFP); a SR/ER retention signal tagged with RFP (AAV9-SR-RFP); an shRNA disruption expression of dynein tagged with RFP (AAV9-*Dnchc1*-shRNA-RFP); and a dominant-negative version of the kinesin-1 tagged with RFP (AAV9-*Kif5B*-DN-RFP). To allow robust expression of fluorescent proteins and shRNA knockdown, experiments were performed at least three weeks after virus injection.

jSR, T-tubule and $[Ca^{2+}]_i$ imaging. To label jSR, paGFP was activated by brief illumination with 405 nm light. To label T-tubules, di-8-ANEPPS was loaded into myocytes as previously described (6). To visualize and acquire paGFP and di-8-ANEPPS fluorescent signals, we used a laser-scanning Olympus FV1000 confocal microscope equipped with an Olympus 60x oil immersion lens. Images were acquired at 1Hz frequency with the Zero-Drift Compensation module engaged, continuously correcting for drifts and thus maintaining a stable focal plane throughout the duration of the experiment. For recordings of TRD-paGFP, each cell was scanned axially and recorded at a plane where the predominant number of TRDs could be seen and tracked. Myocytes were corrected for photobleaching using the Histogram Matching feature of Photo-correction in ImageJ. Cells were analyzed blind to experimental condition via name randomization. Whole-cell $[Ca^{2+}]_i$ transients were measured in myocytes loaded with Fluo-4-AM.

Statistics. Data are presented as COV or mean ± SEM. Two-sample comparisons of normally distributed data were made using a Student's *t* test. A Kruskal-Wallis test was used to compare non-parametric data sets. 'N' represents number of mice used, 'C' and 'S' represent the number of cells and sites analyzed, respectively.

Downloaded from journals.physiology.org/journal/ajpcell at Univ of California Davis (169.237.094.131) on February 4, 2020.

References

1. **Beavers DL, Landstrom AP, Chiang DY, and Wehrens XH**. Emerging roles of junctophilin-2 in the heart and implications for cardiac diseases. *Cardiovasc Res* 103: 198-205, 2014.
2. **Bhabha G, Johnson GT, Schroeder CM, and Vale RD**. How Dynein Moves Along Microtubules. *Trends Biochem Sci* 41: 94-105, 2016.
3. **Cannell MB, and Soeller C**. Numerical analysis of ryanodine receptor activation by L-type channel activity in the cardiac muscle diad. *Biophys J* 73: 112-122, 1997.
4. **De La Mata A, Tajada S, O'Dwyer S, Matsumoto C, Dixon RE, Hariharan N, Moreno CM, and Santana LF**. BIN1 Induces the Formation of T-Tubules and Adult-Like Ca(2+) Release Units in Developing Cardiomyocytes. *Stem Cells* 37: 54-64, 2019.
5. **Drum BM, Dixon RE, Yuan C, Cheng EP, and Santana LF**. Cellular mechanisms of ventricular arrhythmias in a mouse model of Timothy syndrome (long QT syndrome 8). *J Mol Cell Cardiol* 66: 63-71, 2014.
6. **Drum BM, Yuan C, Li L, Liu Q, Wordeman L, and Santana LF**. Oxidative stress decreases microtubule growth and stability in ventricular myocytes. *J Mol Cell Cardiol* 93: 32-43, 2016.
7. **Garbino A, and Wehrens XH**. Emerging role of junctophilin-2 as a regulator of calcium handling in the heart. *Acta Pharmacol Sin* 31: 1019-1021, 2010.
8. **Glover L, Quinn S, Ryan M, Pette D, and Ohlendieck K**. Supramolecular calsequestrin complex. *Eur J Biochem* 269: 4607-4616, 2002.
9. **Gomez AM, Valdivia HH, Cheng H, Lederer MR, Santana LF, Cannell MB, McCune SA, Altschuld RA, and Lederer WJ**. Defective excitation-contraction coupling in experimental cardiac hypertrophy and heart failure. *Science* 276: 800-806, 1997.
10. **Jones PP, MacQuaide N, and Louch WE**. Dyadic Plasticity in Cardiomyocytes. *Front Physiol* 9: 1773, 2018.
11. **Louch WE, Hake J, Mork HK, Hougen K, Skrbic B, Ursu D, Tonnessen T, Sjaastad I, and Sejersted OM**. Slow Ca(2)(+) sparks de-synchronize Ca(2)(+) release in failing cardiomyocytes: evidence for altered configuration of Ca(2)(+) release units? *J Mol Cell Cardiol* 58: 41-52, 2013.
12. **Lu H, Ali MY, Bookwalter CS, Warshaw DM, and Trybus KM**. Diffusive movement of processive kinesin-1 on microtubules. *Traffic* 10: 1429-1438, 2009.
13. **Murphy RM, Dutka TL, Horvath D, Bell JR, Delbridge LM, and Lamb GD**. Ca2+-dependent proteolysis of junctophilin-1 and junctophilin-2 in skeletal and cardiac muscle. *J Physiol* 591: 719-729, 2013.
14. **Nath S, Bananis E, Sarkar S, Stockert RJ, Sperry AO, Murray JW, and Wolkoff AW**. Kif5B and Kifc1 interact and are required for motility and fission of early endocytic vesicles in mouse liver. *Mol Biol Cell* 18: 1839-1849, 2007.
15. **Pritchard HAT, Griffin CS, Yamasaki E, Thakore P, Lane C, Greenstein AS, and Earley S**. Nanoscale coupling of junctophilin-2 and ryanodine receptors regulates vascular smooth muscle cell contractility. *Proc Natl Acad Sci U S A* 116: 21874-21881, 2019.
16. **Sato D, Hernandez-Hernandez G, Matsumoto C, Tajada S, Moreno CM, Dixon RE, O'Dwyer S, Navedo MF, Trimmer JS, Clancy CE, Binder MD, and Santana LF**. A stochastic model of ion channel cluster formation in the plasma membrane. *J Gen Physiol* 151: 1116-1134, 2019.
17. **Soeller C, and Cannell MB**. Numerical simulation of local calcium movements during L-type calcium channel gating in the cardiac diad. *Biophys J* 73: 97-111, 1997.
18. **Song LS, Sobie EA, McCulle S, Lederer WJ, Balke CW, and Cheng H**. Orphaned ryanodine receptors in the failing heart. *Proc Natl Acad Sci U S A* 103: 4305-4310, 2006.

Downloaded from journals.physiology.org/journal/ajpcell at Univ of California Davis (169.237.094.131) on February 4, 2020.

19. **Takeshima H, Komazaki S, Nishi M, Iino M, and Kangawa K**. Junctophilins: a novel family of junctional membrane complex proteins. *Mol Cell* 6: 11-22, 2000.
20. **van Oort RJ, Garbino A, Wang W, Dixit SS, Landstrom AP, Gaur N, De Almeida AC, Skapura DG, Rudy Y, Burns AR, Ackerman MJ, and Wehrens XH**. Disrupted junctional membrane complexes and hyperactive ryanodine receptors after acute junctophilin knockdown in mice. *Circulation* 123: 979-988, 2011.
21. **Vega AL, Yuan C, Votaw VS, and Santana LF**. Dynamic changes in sarcoplasmic reticulum structure in ventricular myocytes. *J Biomed Biotechnol* 2011: 382586, 2011.
22. **Wagner E, Lauterbach MA, Kohl T, Westphal V, Williams GS, Steinbrecher JH, Streich JH, Korff B, Tuan HT, Hagen B, Luther S, Hasenfuss G, Parlitz U, Jafri MS, Hell SW, Lederer WJ, and Lehnart SE**. Stimulated emission depletion live-cell super-resolution imaging shows proliferative remodeling of T-tubule membrane structures after myocardial infarction. *Circ Res* 111: 402-414, 2012.
23. **Zhang L, Kelley J, Schmeisser G, Kobayashi YM, and Jones LR**. Complex formation between junctin, triadin, calsequestrin, and the ryanodine receptor. Proteins of the cardiac junctional sarcoplasmic reticulum membrane. *J Biol Chem* 272: 23389-23397, 1997.

Downloaded from journals.physiology.org/journal/ajpcell at Univ of California Davis (169.237.094.131) on February 4, 2020.

Acknowledgements

This work was funded by NIH 5R01HL085686-14.

Downloaded from journals.physiology.org/journal/ajpcell at Univ of California Davis (169.237.094.131) on February 4, 2020.

Figure Legends

Figure 1: TRD-paGFP is expressed in the jSR of ventricular myocytes. **A**: illustration depicting the location of TRD-paGFP on the luminal aspect of the junctional SR (jSR). **B**: Di-8-ANNEPS labeling of the surface sarcolemma and T-tubules in an isolated ventricular myocyte. White box highlights a representative area where high power images are acquired. **C**: higher magnification imaging of the Di-8-ANNEPS labeled ventricular myocyte show labeled T-tubules. After local photoactivation (circular region) of TRD-paGFP with UV light, GFP fluorescence appears along the T-tubules, representing the location of the jSR. **D**: SR-RFP fluorescence is closely opposed to TRD-paGFP after photoactivation.

Figure 2: The junctional SR is mobile at the cardiac dyad. **A**: histogram shows the frequency of T-tubule (TT) and jSR sites (S = 132) and their respective coefficient of variance (COV). TT sites show lower COV values indicating that they are static. jSR sites on the other hand are both static and mobile and can be fit by four Gaussian functions. The calculated threshold for a jSR to be mobile (static mean + 3 SDs) is noted on the histogram as a dotted line. **B-D**: fluorescent intensity plots (arbitrary units; A.U.) of TT fluorescence (red trace) and TRD-paGFP fluorescence (green trace) as a function of time. Blue lines at the beginning of each trace denotes period of photoactivation of TRD-paGFP. Each representative plot demonstrates individual jSR and TT tracking and fluorescent measurements with variable jSR COVs.

Figure 3: The junctional SR displays different modalities for mobility. **A**: top, di-8-ANNEPS labeled T-tubules (TT) in a ventricular myocyte. White box indicates zoomed region. Middle, after photoactivation with UV light, TRD-paGFP fluorescence is localized to T-tubules. Bottom, during time-lapse imaging, TRD-paGFP fluorescence changes and TT fluorescence is static. **B**: representative images of jSR mobility. In the example retraction images, a region of TRD-paGFP fluorescence disappears from the focal plane, whilst TT fluorescence in the same region remains. During emergence events, distinct regions within the focal plane increase in fluorescence over time. Split events represent the minority of jSR mobility and are characterized as an area of TRD fluorescence once a single unit is divided into two distinct regions over time.

Figure 4: Dynein and kinesin-1 regulate jSR mobility. **A**: Scatter plot of the COV of individual jSR sites from cells expressing *Dnchc1*-shRNA (S = 100) or *Kif5b*-DN (S = 93) versus their respective WT controls (*Kif5b*-WT: S = 166; *Dnchc1*-WT: S = 148). Horizontal red lines in the plots mark the median and range of the data in each group. *P < 0.05; Kruskal-Wallis test. **B**: $[Ca^{2+}]_i$ transients recorded from Fluo-4-AM loaded ventricular myocytes have a higher amplitude and variance in *Kif5b*-WT vs. *Kif5B*-DN myocytes. Data presented as mean ± SEM. *P < 0.05; Student's unpaired *t* test.

Movie 1: Movie showing a 3D spatiotemoral map of paGFP fluorescence in a ventricular myocyte before and after photoactivation with UV light. Time-lapse images show stable and unstable jSR segments.

Downloaded from journals.physiology.org/journal/ajpcell at Univ of California Davis (169.237.094.131) on February 4, 2020.

A.

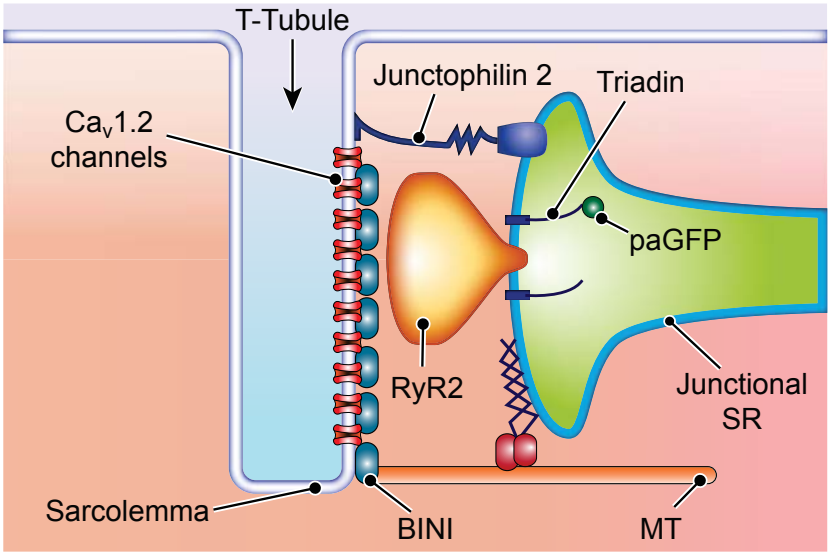

B. Di-8-ANNEPS (surface sarcolemma and T-tubules)

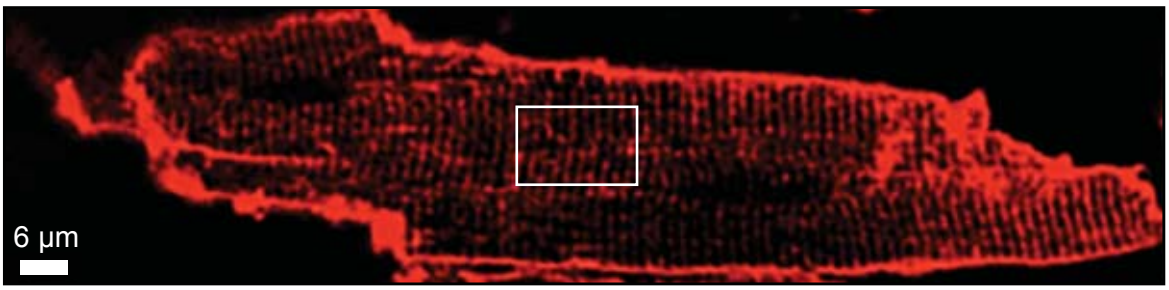

C.

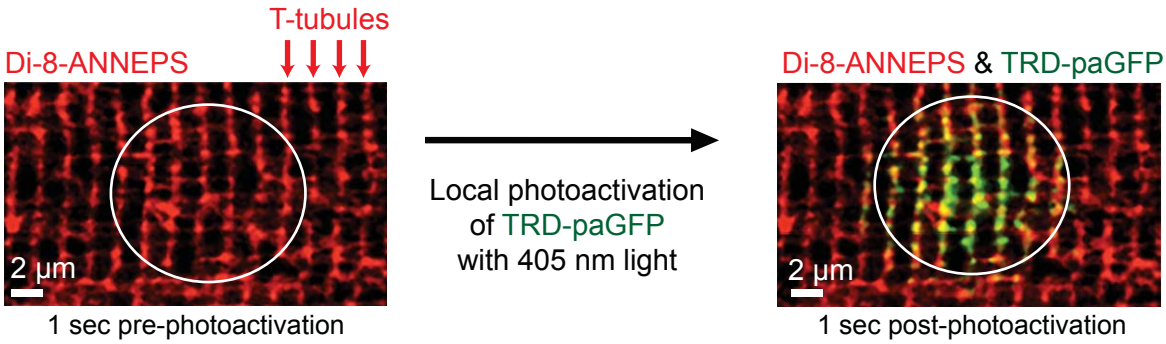

D.

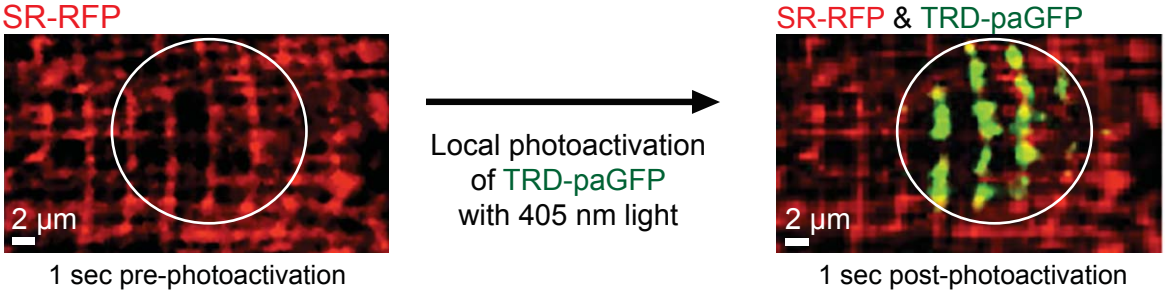

Figure 1

Downloaded from journals.physiology.org/journal/ajpcell at Univ of California Davis (169.237.094.131) on February 4, 2020.

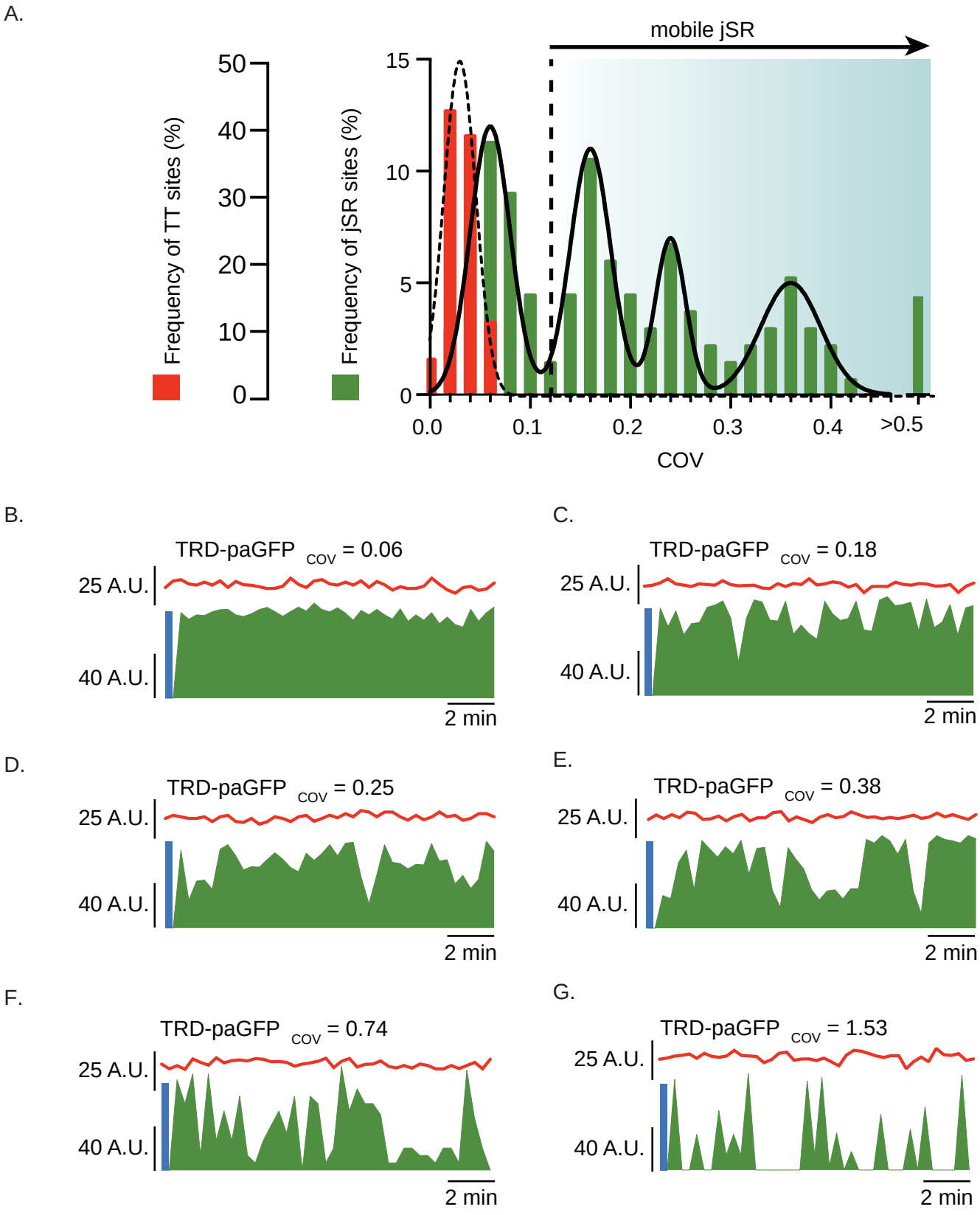

Figure 2

Downloaded from journals.physiology.org/journal/ajpcell at Univ of California Davis (169.237.094.131) on February 4, 2020.

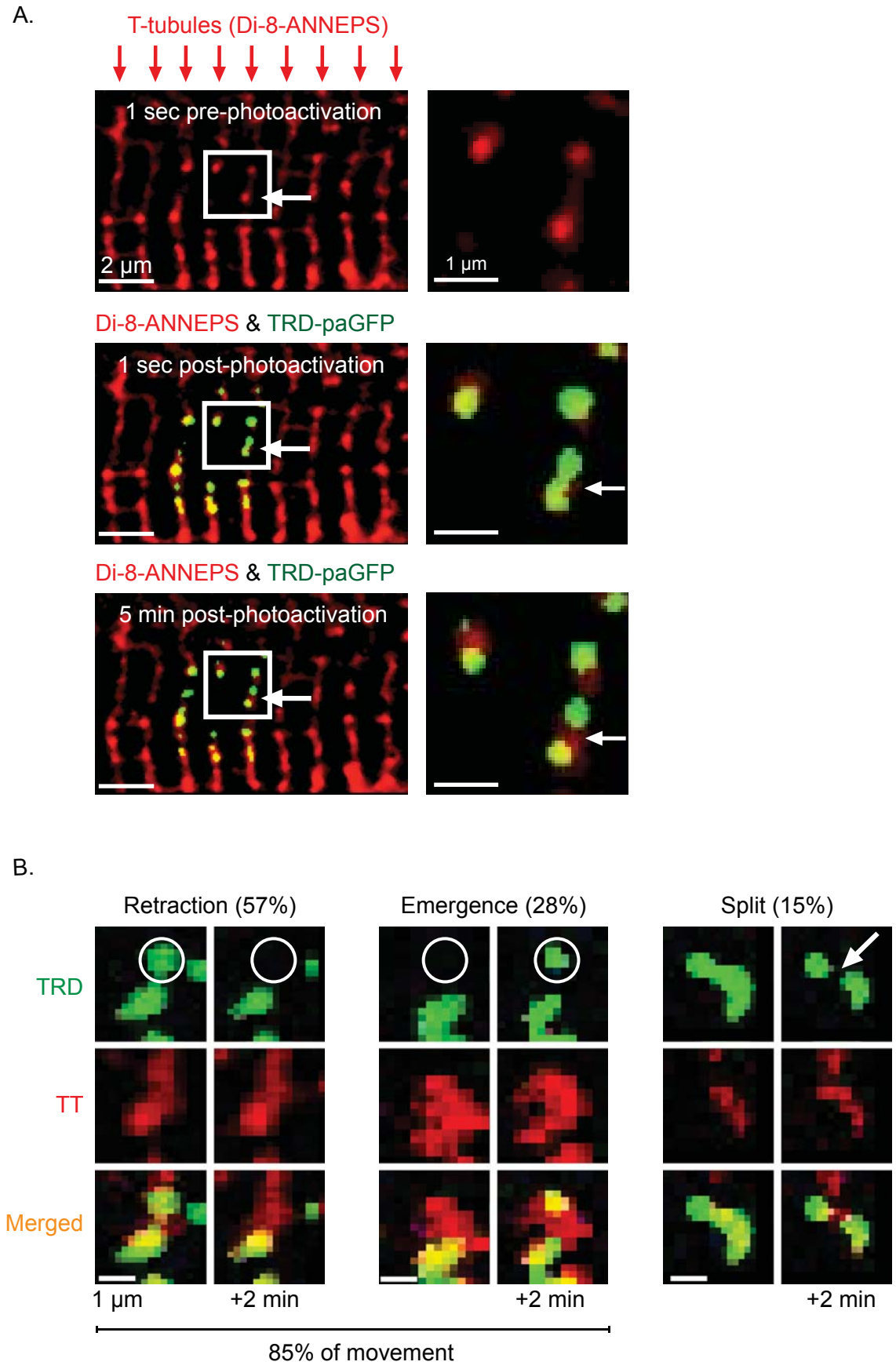

Figure 3

Downloaded from journals.physiology.org/journal/ajpcell at Univ of California Davis (169.237.094.131) on February 4, 2020.

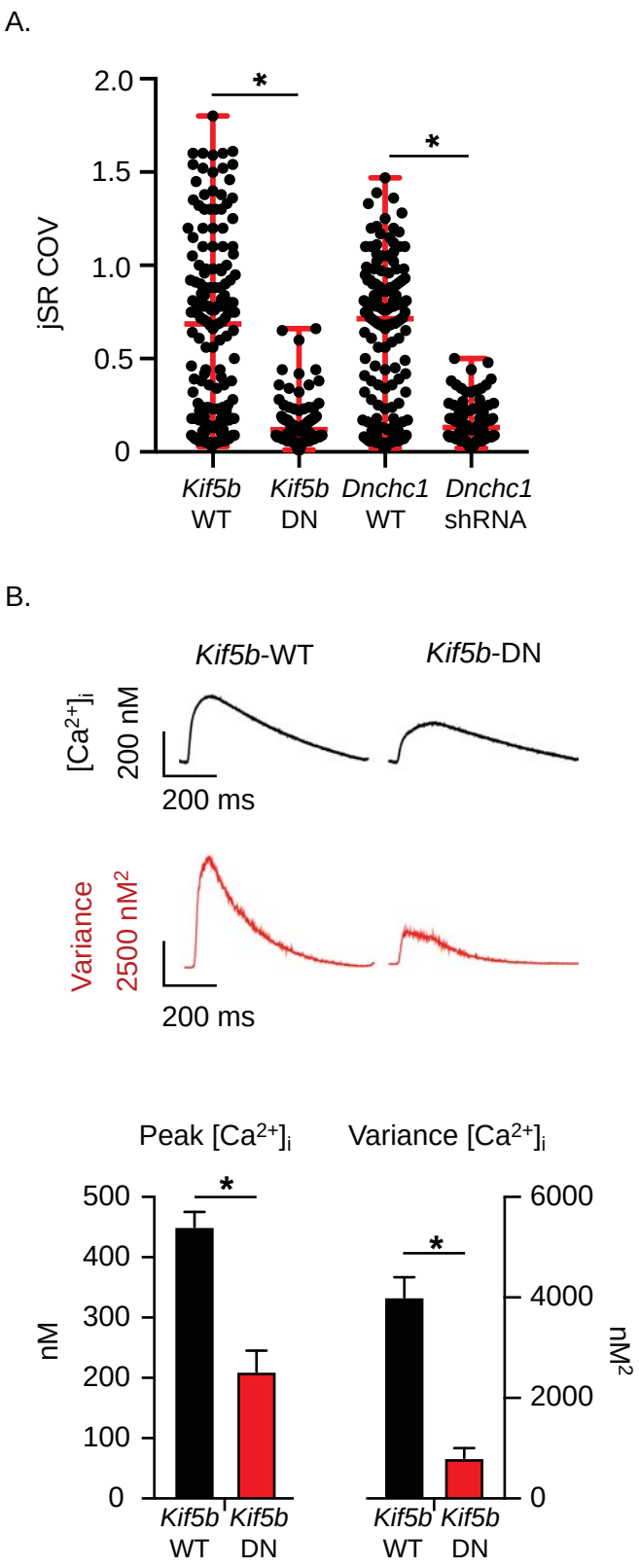

Figure 4

Downloaded from journals.physiology.org/journal/ajpcell at Univ of California Davis (169.237.094.131) on February 4, 2020.